

tracking [84], action recognition [46, 60, 73], vital-signs [26, 87, 90], speech sensing [52, 55, 77], etc. justifies the practicality of mmWave sensing for daily activity monitoring. However, we observe that current mmWave sensing literature does not address continuous human activity monitoring over a longer time or space in an indoor environment, thereby restricting it from being a pervasive practical solution. We summarize these gaps below.

Gaps: The majority of previous studies [12, 16, 36, 60, 73, 88] have reported a high level of sensing accuracy as the subject is kept within the main lobe ($-15^\circ < \text{radar lobe angle} < 15^\circ$) of the radar's field-of-view (FoV). In practice, however, the indoor movement of a subject can be completely random, and thus, activities cannot be detected when the subject is outside the radar's FoV. Incorporating multiple mmWave radars to track multiple users within the same room will significantly increase the complexity due to the complex interference patterns from multi-path signals over the same or overlapping frequency bands. Furthermore, there are countless activities a user can engage in, ranging from macro activities involving major body movements (like cleaning the room) to micro activities involving lesser body movements (like typing on the phone). Most of the previous works [12, 60, 73] primarily consider macro activities for a single user, which are easy to detect due to the rich doppler patterns in the reflected mmWave signals. Nevertheless, in reality, a subject can perform both macro and micro activities over time, whereas different subjects can work on different things simultaneously. Also, tracking activities from multiple subjects is challenging as household objects and motion artifacts across subjects can cause noise from static and dynamic multi-path reflections.

Motivated by these gaps and empowered by our vision, in this work, we first divide the activity grammar into two subsets – (i) *Macro activities* that involve significant body movements (like *changing clothes*) and (ii) *Micro activities* that need minor movements of body parts (like *typing*). Next, to track users' activities seamlessly, we divide the problem statement into two parts (Figure 2): (i) *localization and tracking* in such a way that multiple users' positions can be tracked in every scenario with a single mmWave radar and (ii) continuous opportunistic *activity monitoring* to distinguish both macro and micro activities. The primary challenges involved in the multi-user localization with a single mmWave radar are: (i) Scenarios when the subject is present inside the room but not within the FoV of the mmWave sensor, (ii) Creation of *zombie* subjects due to multi-path reflections, (iii) Associating subjects based on their Radio Frequency (RF) reflections in scenarios when the users cross each other, and (iv) Blind-spots during multi-user tracking due to occlusions by other subjects. Additionally, for continuous activity monitoring across multiple subjects, detecting both macro and micro-scale activities simultaneously with the same mmWave radar configuration is not feasible. For example, the radar with a high-doppler resolution can capture better micro movements but adds more noise in capturing macro activities. In contrast, low-doppler resolution can capture macro movements but fails to detect micro activities.

Contributions: To mitigate these challenges, in this work, we propose *MARS*, a mmWave-based sensing system: **M**ulti-user **A**ctivity tracking via **R**oom-scale **S**ensing. In summary, we contribute in the following ways:

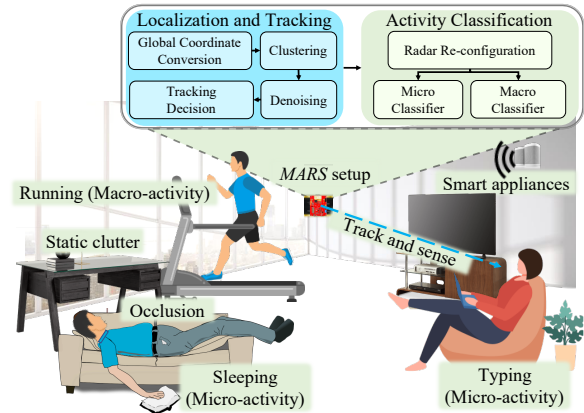


Figure 2: Overview of MARS

- (1) We build an end-to-end prototype for continuous multi-user activity monitoring using a single mmWave Frequency Modulated Continuous Wave (FMCW) radar using a novel technique that rotates and scans full 360° opportunistically. The approach develops methods for dealing with zombies, static clutters, and blind spots utilizing a single rotating radar, thereby avoiding the complex interference patterns that arise from multiple radars.
- (2) *MARS* employs a novel method of differentiated stacking of the captured range-doppler frames as well as opportunistic switching of radar configurations in order to detect macro and micro activities simultaneously. By doing so, to the best of our knowledge, we design a system that can monitor the *highest* number of human activities in the mmWave domain ($1.6\times$ nearest baseline Vid2Doppler [12]). In contrast to the existing works, *MARS* can run on an edge device for real-time monitoring of activities performed by multiple subjects within a room.
- (3) We performed a thorough evaluation of *MARS* at diverse setups and have shown its superiority compared to several other baselines. In classifying the macro and micro activities, we can achieve a weighted F1-Score of 98% and 94%, respectively, with an average response time of $\approx 2s$. We open-source our implementation and sample dataset to reproduce our results: <https://anonymous.4open.science/r/MARS/>.

2 PRELIMINARIES AND PILOT STUDY

2.1 Preliminaries

The primary working principle of COTS mmWave radars is centered on FMCW [64] that transmits continuous frequency chirps and performs *dechirp* operation by combining the transmitted signal (TX) with the signal reflected (RX) from objects to create an *Intermediate Frequency* (IF) signal. From this IF signal, we extract (1) *Pointcloud*, a discrete set of points representing the detected objects [68] and (2) *Range*, the distance of the detected objects from the radar.

2.1.1 Range estimation. The distance information between the object and the radar can be obtained by measuring the frequency difference between the reflected and transmitted signals [44]. This

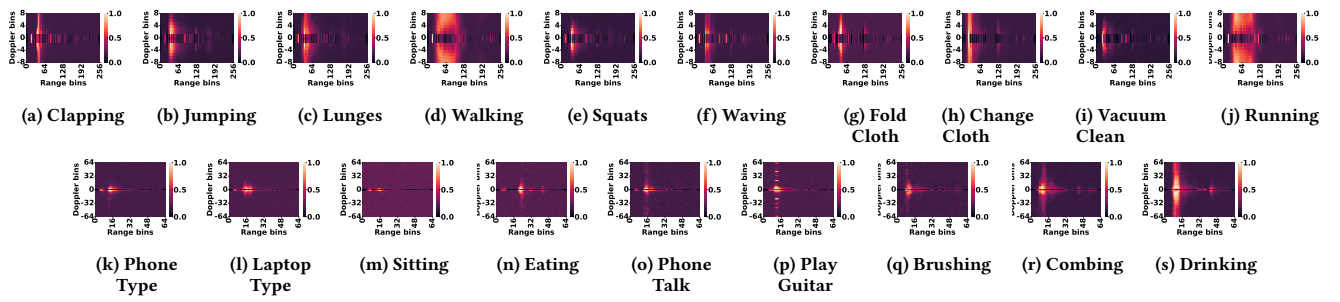


Figure 3: Standard deviation (std) in the range-doppler heatmaps captured during the entire activity duration. (a)-(j): Macro activities with low doppler resolution, (k)-(s): Micro activities with high doppler resolution. Activities having similar body movements have similar patterns, but the difference can be captured in the temporal domain.

frequency gap, also known as *beat frequency* (f_b), arises after a Round Trip Time (RTT) of, say τ . If T_C is the transmit time of the mmWave chirp across a bandwidth of B , then the slope of the FMCW chirp can be given as $S = \frac{B}{T_C} = \frac{f_b}{\tau}$. The RTT delay, τ , can be specified as $\tau = \frac{2d}{c}$ where d is the *distance of the detected object* and c is the *speed of light*. Thus, the detected object's distance can be given as, $d = \frac{c}{2} \cdot \frac{T_C}{B} \cdot f_b$. To calculate f_b , a Fast Fourier Transform (FFT), called *range-FFT*, is performed on the IF signal, which produces frequency peaks at locations where the reflecting object is present. Locating these frequency peaks in turn estimates the range.

2.1.2 Velocity estimation. To measure the velocity of a moving target, the radar transmits N number of chirps separated by a transmission time of T_C . If a subject moves with a speed of v , the phase difference between two successive RX chirps corresponding to the motion, vT_C , can be given as, $\Delta\phi = \frac{4\pi vT_C}{\lambda}$. A second FFT, called *doppler-FFT*, is performed on these phasors to determine the movement or velocity of the object. This information is captured in a 2D matrix called *range-doppler* $\mathbb{D}_{D \times R}$ where D and R correspond to the numbers of *doppler bins* and *range bins*, respectively.

2.1.3 Pointcloud estimation. The pointcloud is estimated through the standard CFAR algorithm [58] that detects peaks of the range-doppler matrix corresponding to the detected objects. The pointcloud consists of the coordinates (x_i, y_i, z_i) , doppler variation (d_i), and the received power (p_i) of the detected objects. The pointcloud set (S) for N number of detected objects can be given as $S = \bigcup_{i=1}^N \{(x_i, y_i, z_i, d_i, p_i)\}$.

2.2 Pilot Study

We consider 19 different activity classes from *Activities of Daily Living* (ADLs), *Instrumental Activities of Daily Living* (IADLs) [9], and *daily indoor exercises* – (i) *macro activities* like walking, running, jumping, clapping, lunges, squats, waving, vacuum cleaning, folding clothes, changing clothes, and (ii) *micro activities* like laptop-typing, phone-talking, phone-typing, sitting, playing guitar, eating food, combing hair, brushing teeth, and drinking water. In contrast to the existing literature that primarily uses voxelized pointcloud [22, 60, 73, 82] or 1D doppler [12, 16], in this paper, we explore range-doppler 2D heatmaps for activity classification; the primary motive

is to find a parameter that can detect both macro and micro activities simultaneously from different users. For this purpose, we conduct a set of *pilot experiments* to explore to what extent range-doppler information can be used in capturing human activity signatures and how the indoor setting impact such sensing capability.

2.2.1 Feasibility study for range-doppler. Figure 3 shows the standard deviation in the range-doppler heatmaps captured during the activity. Notably, standard deviation technique removes static powers (-3 to 2 doppler bins) in the heatmap; thus, we see a low-power value in these doppler bins. We observe that each activity has different signatures captured by the range-doppler heatmap. Although the plotted standard deviation looks similar for some activity pairs with similar body movements (like walking/running, jumping/lunges), there are temporal changes in the heatmaps; for example, “running” induces a faster change than “walking”. Thus, combining the observations from range, doppler, and time, we can get different signatures. Notably, the macro activities have more robust patterns due to the magnitude of movement involved. Even though the micro activities have relatively weaker signatures, they can be distinctively captured with a *higher doppler resolution* (-64 to +64 doppler bins, in contrast to -8 to +8 doppler bins used for macro activities).

2.2.2 Impact of static clutters. Static clutters are any object (walls, furniture, etc.) that are stationary but can reflect the mmWave signal and therefore, generates unwanted signatures in the range-doppler data. We consider a scenario with two subjects – *Subject 1* and *Subject 2*, both sitting inside the room, as shown in Figure 4(a). The room also contains multiple static clutters, such as wooden sheets and walls. From the corresponding range-doppler heatmap, we observe multiple peaks at the range bins corresponding to both the subjects and the static clutters. Indeed, the static clutters produce a higher magnitude along the zero doppler axis, thereby signifying zero or no movement. On the other hand, the dynamic movements of the subjects are positioned across non-zero doppler bins. A major takeaway from the range-doppler heatmap is that static clutters are easily identifiable by their zero-doppler signatures.

2.2.3 The effect of Non Line of Sight (NLoS) movements. To study the NLoS reflections, we first ask a single subject (Subject 1) to stand close to a wall and make some movements (macro-scale) as shown

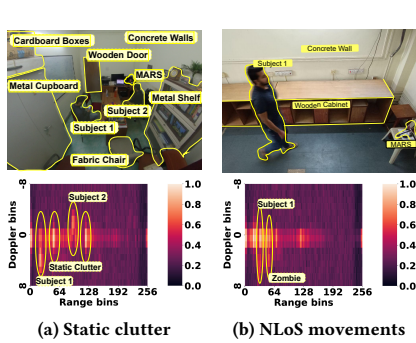


Figure 4: Range-doppler signatures for two scenarios

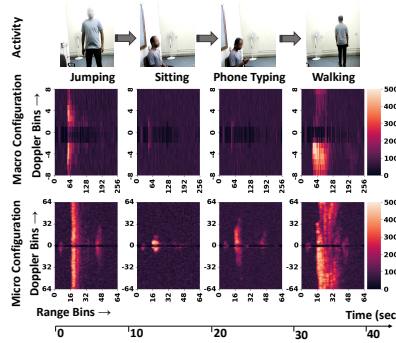


Figure 5: Range-doppler (standard deviation) for individual activity windows over time

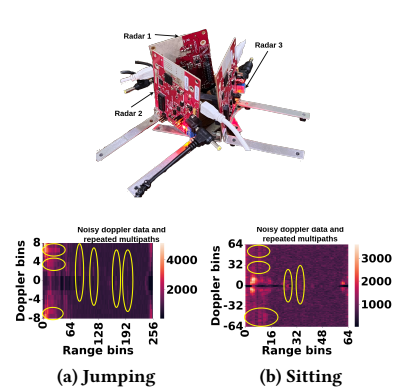


Figure 6: Multi-radar challenges

in Figure 4(b). From the corresponding range-doppler heatmap, it can be observed that the subject’s movements are captured at two different instances at two different range bins. Of the two visible peaks, the more substantial peak belongs to the actual user’s movement, whereas the other instance, also termed as a *zombie subject*, occurs due to the multi-path reflection from the wall.

2.2.4 Impact of radar configurations on determining users’ activity. To understand how the radar configuration affects the patterns in the activity signatures, we ask one subject to switch his activity from jumping to two micro activities, namely, sitting in a chair and phone typing, and finally, walking out of the room. The subject is asked to repeat the pattern twice to collect the corresponding range-doppler data under *low and high doppler resolution*. From the std in the heatmap across the entire activity time axis Figure 5, it is evident that low doppler resolution is adequate for capturing macro activities like walking and jumping. Still, typing and sitting does not have any significant signatures. On changing the radar configuration to *high doppler resolution*, we observe that micro activities like typing and sitting have better visibility. However, with this, the macro activities (walking, jumping) generate noisy data due to the higher resolution. Therefore, *different doppler resolutions* is crucial to capture the signatures corresponding to different activities.

2.2.5 Impact of multiple radars. To have entire room coverage, we have taken three radars and kept them in a colocated position with 120° to each other as shown in Figure 6. We observe that incorporating multiple radars within the same room leads to complex interference patterns in the range-doppler heatmaps. The same or overlapping frequency bands lead to interference in the mmWave chirps and also cause more multipath effects. As shown in Figure 6, the range-doppler heatmaps are very noisy and have complex interference patterns which are not easily separable. This indicates that using multiple radars for 360° coverage makes the system complex; therefore, we need some alternate solution.

3 METHODOLOGY

To have the end-to-end user localization and activity monitoring pipeline, we divide the problem into two sub-problems as highlighted in Figure 7: (i) subject detection followed by the localization

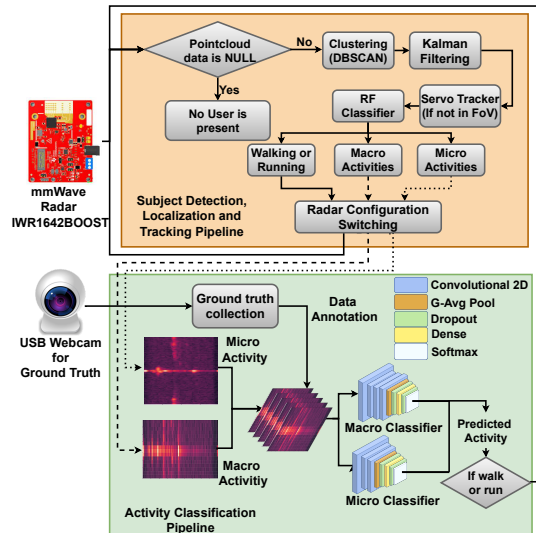


Figure 7: System architecture

and tracking of the subjects, and (ii) activity classification for individual subjects. We next discuss the two modules corresponding to these two sub-problems.

3.1 Localization and Tracking

MARS relies on the *pointcloud data* to localize subjects and track their movements. Motivated by the challenges discussed in Subsection 2.2, we perform the following steps.

3.1.1 Isolate subjects from static clutters. In practice, multiple static objects can be present within the FoV of the radar. As we are interested in identifying subjects’ movement, the background, corresponding to stationary objects, needs to be removed. For this, we remove the zero-valued doppler bins for segregating the static objects (clutters). With this step, the mmWave radar can generate a pointcloud that does not contain static obstacles to isolate the subjects. Once *MARS* starts receiving the pointcloud data, it tracks

the subject by converting its pointcloud coordinate to a global coordinate.

3.1.2 Global Coordinate Conversion. When the subject is present within the room but outside the radar's FoV, localization, and activity recognition of the subject is not feasible. As a solution, we mount the mmWave radar on top of the rotor axis of a servo motor. This enhances the FoV of the radar to 360°. However, rotating the sensor will directly change the reference coordinate system of the estimated pointclouds. Therefore, instead of keeping the local coordinate system w.r.t. the radar, we use a magnetometer to keep a global reference coordinate system. The magnetometer provides the reference azimuthal angle w.r.t. the earth's magnetic pole. Consider a user at $P(x, y)$ in the radar coordinate system as shown in Figure 8. The radar is oriented by an angle of θ w.r.t. the magnetometer. So in the global coordinate system, the angular position of the object is at $(\theta + \phi)$, where $\phi = \tan^{-1}(\frac{y}{x})$. Equation 1 illustrates the transformation of the radar coordinate system to the global coordinate system.

$$\begin{bmatrix} x' \\ y' \end{bmatrix} = \begin{bmatrix} r \cos(\theta + \phi) \\ r \sin(\theta + \phi) \end{bmatrix} = \begin{bmatrix} \cos \theta & -\sin \theta \\ \sin \theta & \cos \theta \end{bmatrix} \begin{bmatrix} x \\ y \end{bmatrix} \quad (1)$$

With the above transformation matrix, the pointclouds are now

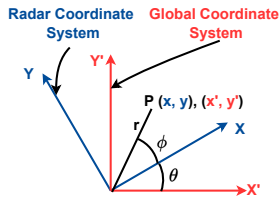


Figure 8: Transformation of the coordinate system

referenced w.r.t. the magnetometer and does not suffer from any coordinate shift due to the rotation of the radar.

3.1.3 Tracking multiple subjects. Based on the pointcloud data, we have information about all the subjects; however, we also get noisy pointclouds due to the movements of the subjects. To tackle this, we take the pointcloud data in a queue format and pass this information to Density-Based Spatial Clustering of Applications with Noise (DBSCAN) [32] for clustering. Each cluster is associated with a unique ID to associate subjects with their respective clusters. Now, to detect the presence of a new subject, *MARS* compares the detected pointcloud clusters between two consecutive frames received from the radar. If the Euclidean distance between the centroid of a cluster over a new frame and that over the previous frame is less than ϵ , we keep the respective cluster ID the same as before. In the case of a newly discovered cluster, we assign it a new cluster ID, indicating a new subject. Note, ϵ is a hyperparameter, and in our setup, we keep it as 10cm, signifying the minimum range resolution for a subject.

3.1.4 Tracking movement of individual subjects. After the clustering step in the pipeline, each cluster corresponds to the pointcloud information associated with each subject. However, some of these clusters may correspond to zombie subjects, as discussed earlier.

We observe that *pointclouds for zombie clusters have a low reflection power* and thus are generated less frequently when compared to the pointclouds caused by the actual subject. So, we first apply a mode function on the pointcloud queue for each cluster to filter out the pointclouds generated more frequently due to the actual subject's presence. The remaining noisy outliers get removed with this approach. However, due to the uncertain movements of the subjects, two subjects may impede each other while crossing. This may lead to *blind spots* in the pointcloud data. We handle such blind spots as follows.

3.1.5 Handling blind spots during multi-user tracking. To track each subject seamlessly, we apply a Kalman filter [61] on the pointcloud queue. The Kalman filtering technique uses the prior knowledge of the state of an object and then *predicts* and *updates* the location and velocity of that object for the next frame. For precise tracking of individual clusters instead of a static Kalman gain, we opted for Recursive Kalman Filter (RKF) to estimate the subjects' motion states. RKF can recursively generate the error covariance matrix and Kalman gain at each stage of the update process. With this step, we can estimate the subjects' state when the actual pointcloud data is unavailable due to occlusion by other subjects' movement or errors in the former pipeline.

3.1.6 Servo-based tracking. Usually, the azimuthal FoV of the radar is 120° which can localize and track subjects. To enhance this FoV, we rely on servo-based tracking. As soon as we have the final coordinates of the denoised pointclouds, we check if each subject is within the main lobe of the radar, i.e., $\leq \pm 15^\circ$. Otherwise, we rotate the servo towards the subject by an angle of $\tan^{-1}(\frac{y}{x})$, to generate high-fidelity pointclouds and range-doppler heatmaps which are needed for activity classification. We stop the rotation when the subject is within $\pm 15^\circ$ so that the doppler remains unaffected for the next activity classification task. Gradually with the rotation process, a new pointcloud queue is generated for subjects that were earlier outside the FoV.

3.1.7 Monitoring state change of a subject. Once a subject is tracked, *MARS* monitors the possible state changes of that subject by utilizing the pointcloud data. Broadly, it performs a high-level classification to check whether (i) the subject is walking or running inside the room or (ii) the subject is static and performing some macro/micro-activities. For this purpose, we capture the mean, standard deviation, kurtosis, and skewness in each of the denoised pointcloud clusters for a time window of 1 seconds. These features are fed to a Random Forest Classifier to predict the subject's activity scale. Based on the prediction, we continue the localization and tracking if the subject is walking or running. Else, *MARS* enables the macro or micro activity classifier opportunistically based on the inference. Thus we name this classifier as Opportunistic Classifier.

3.2 Macro/Micro Activity Monitoring

We keep two different radar configurations to capture the classes of micro and macro activities. For macro activities, *MARS* uses a low doppler resolution of 16 doppler bins (captures major body movements but eliminates the details that may generate noise), while for capturing micro activities, it uses a high doppler resolution of 128 doppler bins (captures minor body movements with finer

details). Using range-doppler enables us to easily switch the radar configurations at different resolutions to recognize both macro and micro activities from different users.

3.2.1 Segregation of individual subject’s activity signatures. As shown in Figure 3, range-doppler is represented as a heatmap image, where the abscissa is the range, the ordinate is the doppler speed containing the power value of subjects’ movement. Each subject’s activity has its activity signatures in the range-doppler heatmap (See Figure 3). To classify the activity of individual subjects, we first segregate these activity signatures based on the range bins. From the pointcloud data (collected along with the range-doppler), we check if there is a non-zero doppler value in the range profile where the subject is present. If a doppler variation exists, we slice out that Range-doppler heatmap information with padding of ± 10 range bins. Additionally, we define another copy of the Range-doppler heatmap for each subject, replacing the remainder with the minimum heatmap value for the subject. In this way, each subject has its own activity signatures, and the remaining signatures corresponding to other subjects are suppressed. This modified range-doppler data is fed to the classification model.

3.2.2 Differentiated frame stacking for macro/micro activities classification. These macro or micro activities span over a short period, affecting range-doppler values temporally. We stack 1 sec range-doppler data to capture temporal features, thus achieving a two-dimensional (2D) multichannel array. However, for macro activities, the doppler resolution is low, resulting in a heatmap of size 16×256 , while for micro activities, the doppler resolution is high, resulting in a heatmap of size 128×64 . This diversity results in different Frames Per Second (FPS) for the range-doppler computation and data transfer. For low-resolution doppler, the FPS is 5, while for the high-resolution doppler, the FPS is 2. Therefore, we stack 5 frames together in the case of the macro activity classifier, while for the micro activity classifier, we stack 2 frames together. This enables us to have the range-doppler for a consistent time period of 1 sec for both scenarios.

3.2.3 Model Architecture. The 2D range-doppler heatmaps have different spatial patterns for each activity. So, we employ a 2D Convolutional Neural Network architecture (2D-CNN). Convolution 2D operation considers the dependency of neighboring spatial values and the temporal relationship of past t ($t = \text{FPS}$) frames. We use four and three 2D convolutional layers with ‘same’ padding and Relu activation for the macro and micro activity classifiers. Next, a global average pooling layer is added to extract the average spatial activation across the entire feature map. Finally, we add two successive dropout and dense layers, where the dropout rate is kept as 20% and 10%, respectively. The last layer outputs a joint probability distribution over all possible activities with a softmax activation (detail in Table 1). Although the subject’s orientation may not impact the detection of macro activities, the micro activities need precise signatures. As we collect the range-doppler at a higher resolution for micro activity classification, it can sense the movements even when the signal strength is low. As a result, the proposed 2D-CNN model can capture micro activities even when the subject is not directly facing the radar.

Table 1: 2D-CNN architecture (M: macro, μ : micro)

CNN Layer	Parameters							
	Kernel		Stride		Channel		Dropout	
	M	μ	M	μ	M	μ	M	μ
Input Layer	-	-	-	-	5	2	-	-
Conv1	2 x 5	3 x 2	1 x 2	2 x 1	32	32	-	-
Conv2	2 x 3	3 x 3	1 x 2	2 x 2	64	64	-	-
Conv3	2 x 3	3 x 3	1 x 2	2 x 2	96	96	-	-
Conv4	2 x 3	-	1 x 2	-	96	-	-	-
G-avg Pool	-	-	-	-	-	-	-	-
Dropout1	-	-	-	-	-	-	20%	20%
Dense1	-	-	-	-	32	32	-	-
Dropout2	-	-	-	-	-	-	10%	10%
Softmax	-	-	-	-	6	6	-	-

3.2.4 Opportunistic Configuration Switching. For each macro and micro activity, MARS switches the configuration accordingly (as derived from the step mentioned in Section 3.1.7). Once the activity classification is performed, it checks whether the subjects are still in their activity state. If any subject starts walking or running, the micro and macro classifiers can detect that and switch the configuration back to capture the pointcloud data to reinitiate the *Localization and Tracking Pipeline*. The clustering and denoising filters get restarted to track the subjects’ movement.

4 IMPLEMENTATION

As shown in Figure 9a, MARS is developed on top of a COTS millimeter wave radar, IWR1642BOOST [4]. The system is tested in three different rooms (see Figure 9b, 9c, 9d) – (i) R1, an office cabin of size $4 \times 3 \text{ m}^2$, (ii) R2, a classroom of size $8 \times 5 \text{ m}^2$, and (iii) R3, a laboratory of size $12 \times 6.5 \text{ m}^2$. The ground truth activity of each subject is manually annotated with the help of the video captured using a USB camera. Overall, MARS consists of: the front-end radar and the backend processing unit. The radar senses data and generates 2D pointclouds and range-doppler heatmaps. These data entries are transferred via a USB cable with a baud rate of 921600 to the backend Raspberry Pi-4 Model B [6] with 1.5GHz Broadcom BCM2711 64bit CPU and 8 GB RAM. We have used Python 3.9.6, TensorFlow v2.10.0, and Scikit-learn v1.1.2 for implementing the macro and micro activity classifiers and the opportunistic Random Forest classifier. The models are trained on an iMac-M1 (with 16 GB primary memory running macOS v12.6 with basekernel version: 21.6.0) and then deployed on the Raspberry Pi-4 for live inference. The training takes 10 minutes for the opportunistic classifier and 20 & 25 minutes for the case of macro and micro classifiers, respectively, with a model size of 7.8 MB, 460 KB, and 334 KB, respectively, for the three cases.

4.1 Hardware setup

4.1.1 Radar Configuration. The IWR1642BOOST radar is configured to use two transmitter and four receiver antennas with frequencies of 77-81 GHz (bandwidth 4 GHz). For the three different use cases, i.e., (i) localization and tracking, (ii) macro activity classification, and (iii) micro activity classification, we have used three different radar configurations (Table 2). For the localization and tracking, we set the frame periodicity as 33.33 millisecond to have 30 FPS to fill the localization queue fast so that clustering and Kalman filter-based tracking can be performed with minimal error. This



Figure 9: (a) MARS hardware setup; and data collection in different rooms: (b) R1 (c), R2 (d), R3

Table 2: Radar configuration

Parameters	Localization	Macro	Micro
Start Frequency	77 GHz		
End Frequency	81 GHz		
Range Resolution (cm)	4.36	12.5	
Maximum Range(m)	9.02	6.4	
Maximum Radial Velocity (m/s)	1	0.64	
Velocity Resolution (m/s)	0.13	0.01	
Azimuthal Resolution (Degree)	14.5°		
Frames per Second	30	5	2
Chirps Per Frame	32		64
ADC Samples per Chirp	256		

configuration provides a range resolution of 4.36 cm, with a maximum unambiguous range of 9.02 m. It can measure a maximum radial velocity of 1 m/s, with a doppler resolution of 0.13m/s. The sensor is set to transmit 32 chirps per frame. We use the same radar configuration for the macro activity classification, except we reduce the FPS to 5 to allow the flow of larger range-doppler heatmaps (matrix of size 16×256) via USB. The doppler resolution is kept at 0.01 m/s for the micro-scale activity classification. The size of the range-doppler heatmap is 128×64 , which supports a frame rate of 2 FPS.

4.1.2 Localization and Tracking Setup. To enhance the radar field-of-view to 360° , we have mounted the radar on top of the rotor axis of a TowerPro MG995 Servo Motor [2], powered using a 1200mAh Li-ion Rechargeable Battery. This enables the localization and tracking of subjects for the entire indoor space. GY-273 Compass Magnetometer Sensor [1] is used to transform the point-cloud coordinates to a global coordinate system, i.e., w.r.t. the earth’s magnetic pole.

4.2 Data Collection Setup

Data collection is carried out for 7 subjects (3 female and 4 male), with ages ranging from 23 to 35, for a total duration of 44 hours across 19 different activity classes (details in 2.2) involving both macro and micro activities. We have experimented over different controlled, semi-controlled, and in-the-wild setups, as we explained later for individual evaluations. To generate the ground truth for localization and tracking pipeline of MARS, we manually marked the positions of users’ movement in the room’s floor map. We asked the users to move in the marked path. We have evaluated the MAE in the marked coordinates and the denoised pointcloud coordinates. Further, we have used *mmWave-Demo-Visualizer* [5] tool, and implemented a patch to extract raw data, containing pointcloud and

range-doppler heatmap under different radar configurations. Annotating the video footage captured via another USB camera installed in the room was done with the help of two volunteers.

4.3 Baseline

We compare MARS activity classifier with three baselines, (i) **Pointcloud-based: RadHAR** [73], which is based on voxelized 3D pointclouds for classifying six macro activities. For developing the baseline, we have collected the 3D pointclouds using a TI IWR1443ISK [8], and we train the classifier (as provided in [73]). (ii) **Range-Doppler: Vid2Doppler** [12], which used range-doppler data to classify 12 different activities. With our collected datasets, we transfer-learn the model weights using the open-sourced Vid2Doppler classifier model. (iii) **VGG-16 network** [72] which is pre-trained on the ImageNet [30] dataset, we apply transfer learning to learn new model weights w.r.t. our collected range-doppler matrix. This transfer learning approach helps in reducing the feature extraction part, as all the trained convolutional layers in VGG-16 are used as feature extractors and do not require retraining. The base VGG-16 model has been enhanced with 2D-Global Average Pooling and successive Dropout and Dense layers as done in the 2D-CNN Architecture (see § 3.2.3). The models are trained with a train-test split of 70%-30% and a validation split of 20% from the training set.

5 EVALUATION

5.1 Overall Performance

We consider three different scenarios to evaluate the overall performance of MARS in comparison to the baselines – (i) single subject, multiple activities over time (*Temporal activity diversity*), (ii) multiple subjects, individual subject performs a single activity over time but different subjects may perform different activities (*Spatial activity diversity*), (iii) multiple subjects, each performing different activities over time (*Spatio-temporal activity diversity*). We performed these experiments in a room R2; later, we discuss the impact of the room size of MARS performance with a *leave one out* train-test method. To evaluate the efficacy, we use two different metrics. We measure the *average number of hits per second*, indicating the rate at which the individual methods are able to correctly report the activity being performed. As the activities are performed in a temporal sequence, this metric indicates the efficacy for real-time prediction of the activities. We also compute the *average response*

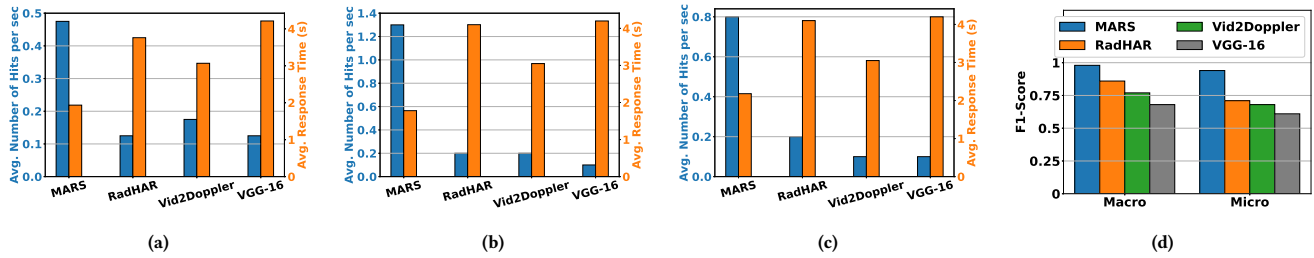


Figure 10: Average number of hits and average response time while predicting (a) different activities over time (single-user), (b) multi-user, (c) different activities over time for multi-user, (d) overall weighted F1-Score of MARS

time, the amount of time a method needs to produce the first correct output after a subject starts performing an activity.

5.1.1 Impact of different activities over time. Here, we asked the subjects to choose four activities (two macro and two micro) in a logical sequence and perform each for at least 10 sec within a room. For example, a subject may first do some exercise through jumping (macro), then sits (micro), then take their phone and type a message (micro), and finally walk to leave the room (macro). As shown in Figure 10(a), *MARS* takes the least response time in inferring the activities with the highest number of hits per second in comparison to the baselines. We observe that the response time for the first activity takes ≈ 2 sec, which involves the bootstrap time to denoise and cluster the data for localizing the subject. When a configuration switch is necessary (macro to micro or vice versa), the average response time is ≈ 3.14 seconds. Without a configuration switch, the average response time is ≈ 1.08 seconds. In comparison, the baselines perform worst in the response time due to more extended frame stacking (2 sec and 3 sec, respectively, for RadHAR and Vid2Doppler) and longer classifier inference time (≈ 4 sec for VGG-16). Longer response times of the baselines directly impact lowering the number of hits in the activity time window, as shown in Figure 10(a) w.r.t. *MARS*, which has a low response time due to smaller frame stacking (1 sec) and reduced inference time (≈ 0.08 sec) with a light-weight model architecture.

5.1.2 Impact of multi-user activities. In the second scenario, we pick four subjects and ask three of them to choose one activity from the set of macro activities and the remaining one to choose one from the set of micro activities. After determining the subjects' location and states, *MARS* configures the low doppler resolution and classifies the macro activities simultaneously with a response time of ≈ 3 s at the beginning. However, using 1 sec of frame-stacked data, it can gradually infer the three macro activities simultaneously with a response time of 1.04s. For the subject performing the micro activity, it switches the configuration to high doppler resolution and classifies the same with a response time of 2.08 sec, resulting in an average response time of 1.9 sec and on an average of 13 hits in the entire activity time window of 10 sec (see Figure 10(b)). RadHAR and Vid2Doppler show poor performance as they are built focused on macro activities only and are trained only for single-user activity classification. Interestingly, we observe that the average number of hits per second for *MARS* is more in this case (spatial

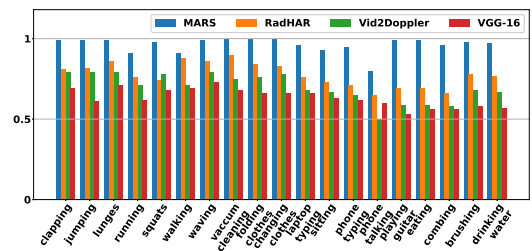


Figure 11: F1-Score across different activities

diversity) compared to the previous one (temporal diversity), as the radar needs less configuration switching.

5.1.3 Impact of different activity over time for multi-user. In the final scenario, we ask four subjects to simultaneously perform four different activities of their choices (with at least one micro activity and one macro activity) in sequence within a room, where they switch the activity in approximately every 10 sec. As shown in Figure 10(c), the average response time of *MARS* in this scenario is ≈ 2 sec with 8 average number of hits, in a time window of 10s. Thus the overall performance of *MARS* demonstrates its potential to be adopted as a real-time system for multi-subject scenarios.

Next, we evaluate individual components of *MARS*, beginning with the Opportunistic Random Forest Classifier.

5.2 Performance of Opportunistic Classifier

With the dataset collected across different scenarios, under the localization configuration (as mentioned in Table 2), we first perform a train-test split of 70% : 30%. The Opportunistic Classifier (as discussed in Sec. 3.1.7) is trained with the 70% training dataset with a validation split of 20% from the training set. According to our observations, the pointcloud dataset can accurately classify macro and micro activity sets with 90%, and 99% accuracy, respectively. However, a slight overlap exists (of 10%) between the macro activity class and the *walking* or *running* class, as under both the scenarios, there exists a significant variation in the pointcloud data. Interestingly, this variation is similar during the activity initiation period, and gradually, the variation becomes more separable with time.

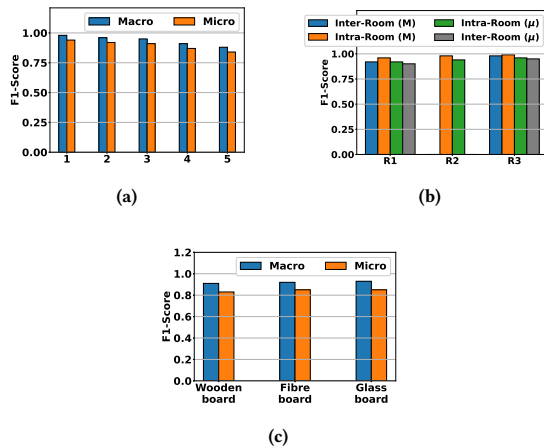


Figure 12: Impact on (a) # of subjects, (b) different rooms (M: macro, μ : micro), (c) different blockages

5.3 Performance of Activity Classifiers

We next evaluate the performance of the macro and the micro activity classifiers w.r.t. the baseline in terms of the weighted F1-Score. As shown in Figure 10(d), the weighted F1-Score for *MARS* is 98% in the case of macro activities and 94% in the case of micro activities. The lower weighted F1-Score for RadHAR is primarily because it relies on the pointcloud dataset for the voxel formation and generates sparse pointclouds in case of micro activities. For Vid2Doppler, the poor accuracy is primarily because it takes only 32 doppler bins which are unsuitable for micro activity monitoring, and the model feature extraction part is pre-trained on macro activity datasets. As the body movements in the case of macro activities are significant, thus the classifier can segregate individual classes with an excellent weighted F1-Score (close to ≈ 0.98). In the case of the micro activities, the body movements are less significant, but with the proposed classification pipeline with a higher doppler resolution, we can achieve a weighted F1-Score of 0.94. Among the micro activities, laptop typing, eating food, and playing guitar involve higher body movements, and thus for these particular activities, we observe higher F1-Score (see Figure 11). Activities such as sitting, typing, and talking on a phone are carried out while subjects sit on a chair. Thus, the doppler shift for these activities is very low, and minimal variation exists compared to other micro activities. When the subject talks on a phone, the overlap with the *sitting* class is more significant ($\approx 10\%$). In Figure 11 we show activity wise F1-Score of *MARS* w.r.t. the baselines. In [73] authors have considered only five activities, and for Vid2Doppler [12] 12 activities are considered, while in our case with a total of 19 activities, the classification F1-Score of the baselines significantly drops in comparison to *MARS*. We look deeper at the activity classification pipeline of *MARS* with the micro benchmarks detailed below.

5.4 Results: Micro Benchmarks

5.4.1 Impact of number of subjects. In Figure 12(a), we show the variation in the weighted F1-Score for both the macro and micro

activity classifiers with the different number of subjects present inside the room. With an increase in the number of subjects up to 5, we observe a direct impact on the weighted F1-Score for both macro and micro classifiers, but by only 10%.

5.4.2 Impact on different rooms. We studied *MARS* extensively in the three rooms R1, R2, R3 as discussed in Sec. 4. We consider two cases – (i) *Inter-room Training*, where we train *MARS* over the data collected at R2 and test over R1 and R3, and (ii) *Intra-room Training*, where we train and test the models using the data collected over the same room. As shown in the Figure 12(b), the weighted-F1 Score for all the rooms is $> 90\%$ for both the classifiers. Interestingly, for R1, the multipath-reflection effect is more significant due to the smaller room size, so the F1-Score is lower; however, the impact of intra-room and inter-room is not very significant as *MARS* learns the features related to the doppler patterns of the subject’s activity rather than room-specific features. Inter-room training and testing (leave one out) also indicate that the model does not **overfit** on datasets.

5.4.3 Impact of blockages. We have tested *MARS* with different blockages such as (i) Wooden board, (ii) Fibreboard, (iii) Glass board, etc. However, mmWave at higher frequency shows higher penetration loss, although it can penetrate materials like plywood, glass, and fiber. Thus for macro activities, at least, we can achieve weighted-F1 Score $> 90\%$ (see Figure 12(c)). However, the F1-Score for micro activities is lower, as small phase variations are attenuated more quickly than macro phase variations.

5.4.4 Impact of subject orientation. We test *MARS* under different body orientations of the subject, i.e., (i) front, (ii) left, (iii) right, (iv) back, w.r.t. the setup. As observed in Figure 13(a) under different body orientations, the macro activity classifier can recognize the activity class with a weighted F1-Score of ≈ 0.98 . But in the case of the micro activity classifier (shown in Figure 13(b)), the weighted F1-Score is lower, especially for the case of phone talking. During talking on the phone, the subject’s body orientation, such as back or right (while holding the phone in left hand) concerning the radar, significantly impacts the activity classification due to the occlusion of small-scale body movements. Nevertheless, it is comforting to see that for other micro-activities, the weighted F1-score is always > 0.80 , even when the subject is at a complete opposite orientation from the radar.

5.4.5 Impact of distance. Figure 13(c) shows the variation in the weighted F1-Score for the macro activity classifier under different distances from the subject. The classification is reported for up to a distance of 5m. The average weighted F1-Score is ≈ 0.98 as observed. However, Figure 13(d) indicates that the F1-Score for micro activity classifier sometime drops (up to 10%) with the increase in the distance. Due to signal attenuation, the doppler shift for micro activities sometimes becomes undetectable with increasing distance. Interestingly, the macro activities provide better results with higher distance ($>3m$, as shown in Figure 13c), since the spread of macro body movements can be easily captured within radar’s conical FoV with the increased distance.

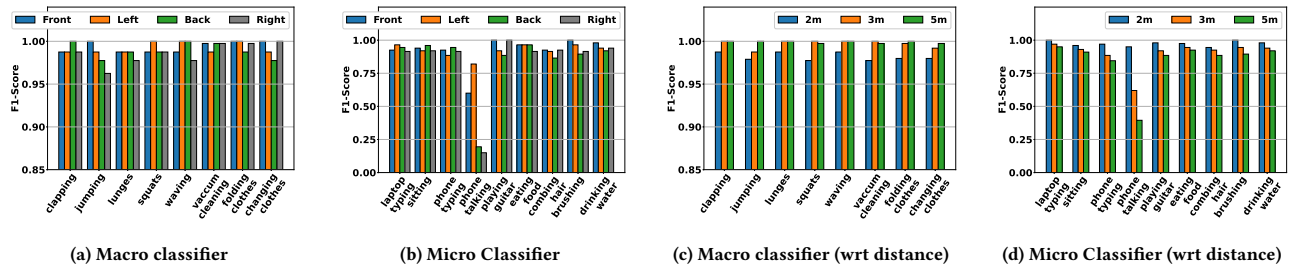


Figure 13: Weighted F1-Score at different orientations

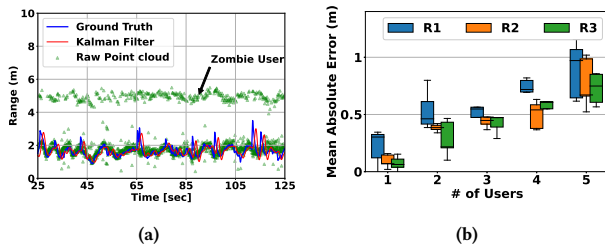


Figure 14: (a) Qualitative analysis of Kalman tracking pipeline, (b) MAE with different walking subjects

5.5 Localization and Tracking Performance

Figure 14(a) shows a snapshot of the subject tracking pipeline with respect to the ground truth distance. In this selected experiment, we observe the raw pointcloud data for the subject cluster contains the signature of a zombie subject arising due to multi-path reflections (present at a distance of $\approx 5m$). With the proposed localization approach, this zombie subject’s pointcloud gets suppressed. In Figure 14(b), we show the mean absolute error (MAE) in subject localization in three different rooms R1, R2, R3, w.r.t. the ground truth under different numbers of subjects present inside the room, who are walking simultaneously within the FoV of the radar at an average speed of 0.7-1.1 m/s. Although the MAE in the localization is < 60 cm with three simultaneous subjects, the MAE gradually increases with increasing the number of subjects walking simultaneously. Since R1 is smaller, the MAE is higher because the pointcloud data is noisier with more multi-path reflections. However, it is comforting to see that even with the five users walking randomly at the normal to moderately high speed, the MAE is within $\approx 1m$.

5.6 Resource and Energy Benchmarks

We measure the resource and energy consumption of the back-end processing unit, i.e., RPi-4, under different scenarios. As observed in Figure 15(a), 15(b), the CPU and the memory utilization in case of the localization and the tracking pipeline is low when the subject is not present inside the room. As the subject enters the room, the Opportunistic classifier gets initiated. As a result of feature computation and pipeline initiation, we observe significantly higher CPU and memory utilization. After that, when the activity classification pipeline gets initiated, we observe that memory utilization increases

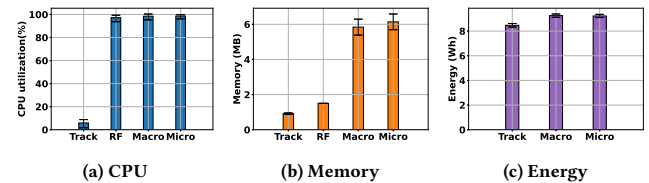


Figure 15: Resource consumption of MARS

Table 3: Comparison of the state-of-the-art systems

Title	Macro Activities	Micro Activities	Continuous Monitoring	Real-time Inference	Multi-Person Monitoring
IMU2Doppler [16]	✓	×	✓	×	×
Mobi2Sense [91]	✓	✓	×	✓	✓
RF-Action [53]	✓	✓	×	✓	✓
RF-Net [31]	✓	×	×	×	×
RF-Pose [93]	✓	×	✓	×	✓
Vibrosight [92]	✓	×	×	×	×
Vid2Doppler [12]	✓	×	✓	✓	×
RadHAR [73]	✓	×	✓	×	×
m-activity [82]	✓	×	×	×	×
RF-Diary [33]	✓	×	✓	×	×
Jiang et al. [46]	✓	×	×	×	×
Cominelli et. al. [29]	✓	×	×	×	×
MARS	✓	✓	✓	✓	✓

significantly due to large-scale feature computation and loading of the trained model in the memory. Finally, using a Monsoon Power Monitor [7], we measure the overall energy consumption of the RPi under the three scenarios – (i) localization and tracking, (ii) macro activity classification, (iii) micro activity classification. As observed in Figure 15(c), the energy consumption is comparatively higher in the case of macro and the micro activity classification because of the higher CPU and RAM utilization.

6 RELATED WORK

Some studies have used wearables for active sensing techniques, mostly to detect human activity [23, 35, 49, 66]. Even though such methods are useful, they are not seamless and pervasive enough. While vision-based activity assessments such as [21, 27, 40, 41, 57] rely primarily on video data, these methods have operational limitations due to LoS issues, occlusions, and privacy concerns. Our next discussion explores alternative passive sensing methods, mainly those based on acoustics and radio frequency.

Acoustic-based: Passive acoustic sensing [51, 79, 80] involves the creation of audio chirps that are reflected away from nearby surfaces and detected by a *microphone*. In this direction, both macro [17], as well as micro activities [51], were studied. Acoustic-based sensing involves several frequencies, including ultra-sounds [46]. Due to the reliance on audio frequency, acoustic-based approaches are susceptible to environmental noise, interference, and microphone orientation. In addition, multiple individuals affect the acoustic signature in an unpredictable manner [14, 80].

RF-based: Radio-frequency (RF) in the form of Wi-Fi [31, 81], RFIDs [47], UWB radars [20, 91] has been studied for capturing human dynamics. Many have explored Wi-Fi Channel State Information (CSI) [29, 29, 74, 75, 81]; as the phase and amplitude of radio waves are impacted by the movements of objects in their path [25]. Both macro and micro-level [13] activities have been studied in this direction. Alternatively, UWB is suitable for penetrating walls [95] and capturing movements [26] including small movements [91]. In some cases, RFIDs are used to capture human activity [43, 62].

Regarding Wi-Fi, CSI extraction from signals is usually a complex process. Other environmental dynamics, such as door movement, furniture movement, and electromagnetic interference, can also affect the signal. Some works [33, 93] rely on FMCW techniques with specialized hardware aiming for a relatively higher depth resolution [33]. However, this specialized hardware is usually expensive compared to COTS hardware [24]. A COTS FMCW mmWave sensor such as IWR1642 [15] demonstrates a better range resolution as compared to the specialized device used in [33] (~3.75cm vs. ~8cm) [33, 63]. Compared to Wi-Fi CSI, UWB has a higher achievable resolution [24]; however, it has a well-known spectrum coexistence issue. RFIDs also have a limited range of around 5 meters. Instead, mmWave-based sensors can detect small movements at a finer level. Due to its shorter wavelength, mmWave can create stronger reflections even from smaller objects [46]. The works [16, 36, 37, 56, 69–71, 73, 82, 86] employing this modality usually rely on emitted mmWave signals in the form of chirps and exploit the received signal reflected by the surroundings to capture activity signatures. COTS mmWave radars often use FMCW chirps for this purpose. Features, such as pointclouds [73, 82], range-doppler [12, 16, 69, 70, 89], etc., have been proven to be effective in movement detection.

In contrast to previous works, this work uses mmWave sensing to continuously track activities since it is minimally intrusive on privacy and captures micro-movements. The single modality is sufficient for continuous activity monitoring of multiple individuals. Our approach also detects the most number of activities (both macro and micro simultaneously) in the mmWave domain with a dynamic environment when multiple users are present. Table 3 highlights the advantages of MARS compared to the state-of-the-art contributions in the relevant domain.

7 CONCLUSION

We need simple yet effective ways for humans to interact with our smart spaces. Existing ideas, however, use techniques that are both invasive and difficult to integrate. The key insight prompted us to design and develop MARS, a lightweight yet highly effective mmWave-based continuous activity monitoring system. Through

experiments, MARS proves its effectiveness of single subject tracking with a mean absolute error of just 45cm despite supporting global coordinates. After that, it demonstrates field-deployable accuracy of 98% and 94%, respectively, for multiple macro and micro-scale activities. Based on the results, we are confident that MARS will seamlessly adapt to human activities in all situations encountered in real-world scenarios.

MARS can be upgraded to a higher resolution by using devices like DCA1000EVM [3]; however, it will lead to higher latency because of the increased volume of data. The existing form of MARS is incapable of capturing micro activities beyond five meters due to signal attenuation with an increasing range, which is a fundamental challenge in mmWave. Instead of limiting our evaluation to a simplistic functional accuracy, we evaluated the performance of MARS based on different counts, orientations, distances, and even energy consumption footprints, comparing it to the state-of-the-art baselines which demonstrate its superiority.

REFERENCES

- [1] 2011. Robodo SEN40 GY-273 HMC5883L Module Triple Axis Compass Magnetometer Sensor Module for Arduino. <https://www.amazon.in/Robodo-Electronics-SEN40-HMC5883L-Magnetometer/dp/B0787LH8XR>. [Accessed September 22, 2023].
- [2] 2013. Tower Pro MG995 Servo Motor. <https://www.towerpro.com.tw/product/mg995/>. [Accessed September 22, 2023].
- [3] 2018. DCA1000EVM. <https://www.ti.com/tool/DCA1000EVM>. [Accessed September 22, 2023].
- [4] 2018. IWR1642BOOST. <https://www.ti.com/tool/IWR1642BOOST>. Accessed September 22, 2023.
- [5] 2018. mmWave Demo Visualizer — dev.ti.com. https://dev.ti.com/gallery/view/mmwave/mmWave_Demo_Visualizer/. [Accessed September 22, 2023].
- [6] 2019. Raspberry Pi 4 Model-B. <https://www.raspberrypi.com/products/raspberrypi-4-model-b/>. [Accessed September 22, 2023].
- [7] 2020. High Voltage Power Monitor | Monsoon Solutions . <https://www.msoon.com/high-voltage-power-monitor>.
- [8] 2020. IWR1443BOOST. <https://www.ti.com/tool/IWR1443BOOST>. Accessed September 22, 2023.
- [9] 2022. ADLs-IADLs. <https://betterhealthwhileaging.net/what-are-adls-and-iadls/>. [Accessed September 22, 2023].
- [10] Fadel Adib and Dina Katabi. 2013. See through walls with WiFi!. In *Proceedings of the ACM SIGCOMM 2013 conference on SIGCOMM*. 75–86.
- [11] Fadel Adib, Hongzi Mao, Zachary Kabelac, Dina Katabi, and Robert C Miller. 2015. Smart homes that monitor breathing and heart rate. In *Proceedings of the 33rd annual ACM conference on human factors in computing systems*. 837–846.
- [12] Karan Ahuja, Yue Jiang, Mayank Goel, and Chris Harrison. 2021. Vid2Doppler: Synthesizing Doppler radar data from videos for training privacy-preserving activity recognition. In *Proceedings of the 2021 CHI Conference on Human Factors in Computing Systems*. 1–10.
- [13] Kamran Ali, Alex X Liu, Wei Wang, and Muhammad Shahzad. 2015. Keystroke recognition using wifi signals. In *Proceedings of the 21st annual international conference on mobile computing and networking*. 90–102.
- [14] Yang Bai, Li Lu, Jerry Cheng, Jian Liu, Yingying Chen, and Jiadi Yu. 2020. Acoustic-based sensing and applications: A survey. *Computer Networks* 181 (2020), 107447.
- [15] Dennis Barrett, Dan Wang, Adeel Ahmad, and Vaibhav Mahimkar. 2017. Using mmWave sensors to enhance drone safety and productivity. *Texas Instruments white paper SPYY001* (2017).
- [16] Sejal Bhalla, Mayank Goel, and Rushil Khurana. 2021. IMU2Doppler: Cross-Modal Domain Adaptation for Doppler-based Activity Recognition Using IMU Data. *Proceedings of the ACM on Interactive, Mobile, Wearable and Ubiquitous Technologies* 5, 4 (2021), 1–20.
- [17] Gaddi Blumrosen, Ben Fishman, and Yossi Yovel. 2014. Noncontact wideband sonar for human activity detection and classification. *IEEE Sensors Journal* 14, 11 (2014), 4043–4054.
- [18] Carlos Bocanegra, Mohammad A Khojastepour, Mustafa Y Arslan, Eugene Chai, Sampath Rangarajan, and Kaushik R Chowdhury. 2020. RFGo: a seamless self-checkout system for apparel stores using RFID. In *Proceedings of the 26th Annual International Conference on Mobile Computing and Networking*. 1–14.
- [19] Leonardo Bonanni, Chia-Hsun Lee, and Ted Selker. 2005. CounterIntelligence: Augmented reality kitchen. In *Proc. CHI*, Vol. 2239. Citeseer, 45.
- [20] Kevin Bouchard, Julien Maitre, Camille Bertuglia, and Sébastien Gaboury. 2020. Activity recognition in smart homes using UWB radars. *Procedia Computer*

- Science* 170 (2020), 10–17.
- [21] Fabian Caba Heilbron, Victor Escorcia, Bernard Ghanem, and Juan Carlos Nieves. 2015. ActivityNet: A large-scale video benchmark for human activity understanding. In *Proceedings of the IEEE conference on computer vision and pattern recognition*. 961–970.
- [22] Pingping Cai and Sanjib Sur. 2023. MilliPCD: Beyond Traditional Vision Indoor Point Cloud Generation via Handheld Millimeter-Wave Devices. *Proceedings of the ACM on Interactive, Mobile, Wearable and Ubiquitous Technologies* 6, 4 (2023), 1–24.
- [23] Pierluigi Casale, Oriol Pujol, and Petia Radeva. 2011. Human activity recognition from accelerometer data using a wearable device. In *Iberian conference on pattern recognition and image analysis*. Springer, 289–296.
- [24] Zhe Chen, Chao Cai, Tianyue Zheng, Jun Luo, Jie Xiong, and Xin Wang. 2021. RF-based human activity recognition using signal adapted convolutional neural network. *IEEE Transactions on Mobile Computing* 22, 1 (2021), 487–499.
- [25] Zhenghua Chen, Le Zhang, Chaoyang Jiang, Zhiguang Cao, and Wei Cui. 2018. WiFi CSI based passive human activity recognition using attention based BLSTM. *IEEE Transactions on Mobile Computing* 18, 11 (2018), 2714–2724.
- [26] Zhe Chen, Tianyue Zheng, Chao Cai, and Jun Luo. 2021. MoVi-Fi: Motion-robust vital signs waveform recovery via deep interpreted RF sensing. In *Proceedings of the 27th Annual International Conference on Mobile Computing and Networking*. ACM, 392–405.
- [27] Shinko Y Cheng, Sangho Park, and Mohan M Trivedi. 2005. Multiperspective thermal IR and video arrays for 3D body tracking and driver activity analysis. In *2005 IEEE Computer Society Conference on Computer Vision and Pattern Recognition (CVPR'05)-Workshops*. IEEE, 3–3.
- [28] Adrian Clark, Andreas Dünser, Mark Billinghurst, Thammathip Piumsomboon, and David Altimira. 2011. Seamless interaction in space. In *Proceedings of the 23rd Australasian Computer-Human Interaction Conference*. 88–97.
- [29] Marco Cominelli, Francesco Gringoli, and Francesco Restuccia. 2023. Exposing the CSI: A Systematic Investigation of CSI-based Wi-Fi Sensing Capabilities and Limitations. In *Proceedings of the 21st International Conference on Pervasive Computing and Communications (PerCom '23)*. 81–90.
- [30] Jia Deng, Wei Dong, Richard Socher, Li-Jia Li, Kai Li, and Li Fei-Fei. 2009. Imagenet: A large-scale hierarchical image database. In *2009 IEEE conference on computer vision and pattern recognition*. Ieee, 248–255.
- [31] Shuya Ding, Zhe Chen, Tianyue Zheng, and Jun Luo. 2020. RF-net: A unified meta-learning framework for RF-enabled one-shot human activity recognition. In *Proceedings of the 18th Conference on Embedded Networked Sensor Systems*. 517–530.
- [32] Martin Ester, Hans-Peter Kriegel, Jörg Sander, Xiaowei Xu, et al. 1996. A density-based algorithm for discovering clusters in large spatial databases with noise.. In *kdd*, Vol. 96. 226–231.
- [33] Lijie Fan, Tianhong Li, Yuan Yuan, and Dina Katabi. 2020. In-home daily-life captioning using radio signals. In *European Conference on Computer Vision*. Springer, 105–123.
- [34] Xiaoyi Fan, Wei Gong, and Jiangchuan Liu. 2018. Tagfree activity identification with rfid. *Proceedings of the ACM on Interactive, Mobile, Wearable and Ubiquitous Technologies* 2, 1 (2018), 1–23.
- [35] Tatsuhiko Fujimoto, Hiroshi Nakajima, Naoki Tsuchiya, Hideya Marukawa, Kei Kuramoto, Syoji Kobashi, and Yutaka Hata. 2013. Wearable human activity recognition by electrocardiograph and accelerometer. In *2013 IEEE 43rd international symposium on multiple-valued logic*. IEEE, 12–17.
- [36] Peixian Gong, Chunyu Wang, and Lihua Zhang. 2021. Mmpoint-GNN: graph neural network with dynamic edges for human activity recognition through a millimeter-wave radar. In *2021 International Joint Conference on Neural Networks (IJCNN)*. IEEE, 1–7.
- [37] Tianbo Gu, Zheng Fang, Zhicheng Yang, Pengfei Hu, and Prasant Mohapatra. 2019. MmSense: Multi-person detection and identification via mmWave sensing. In *Proceedings of the 3rd ACM Workshop on Millimeter-wave Networks and Sensing Systems*. 45–50.
- [38] Xiaonan Guo, Bo Liu, Cong Shi, Hongbo Liu, Yingying Chen, and Mooi Choo Chuah. 2017. WiFi-enabled smart human dynamics monitoring. In *Proceedings of the 15th ACM Conference on Embedded Network Sensor Systems*. 1–13.
- [39] Gaya Hacıane, Rassaniya Lerdpayakkarat, Papat Meteeekotchadet, Juliana Kutch, Jon Roschke, and Hakan Kutgun. 2018. Comma. ai Marketing Plan. (2018).
- [40] Ju Han and Bir Bhanu. 2005. Human activity recognition in thermal infrared imagery. In *2005 IEEE Computer Society Conference on Computer Vision and Pattern Recognition (CVPR'05)-Workshops*. IEEE, 17–17.
- [41] Michael Harville and Dalong Li. 2004. Fast, integrated person tracking and activity recognition with plan-view templates from a single stereo camera. In *Proceedings of the 2004 IEEE Computer Society Conference on Computer Vision and Pattern Recognition, 2004. CVPR 2004., Vol. 2*. IEEE, II–II.
- [42] HexiWear. [n. d.]. HexiWear. <https://www.mikroe.com/hexiwear>
- [43] Anna Huang, Dong Wang, Run Zhao, and Qian Zhang. 2019. Au-id: Automatic user identification and authentication through the motions captured from sequential human activities using rfid. *Proceedings of the ACM on Interactive, Mobile, Wearable and Ubiquitous Technologies* 3, 2 (2019), 1–26.
- [44] Cesar Iovescu and Sandeep Rao. 2020. The fundamentals of millimeter wave radar sensors. *Texas Instruments* (2020).
- [45] Jesse V Jacobs, Lawrence J Hettlinger, Yueng-Hsiang Huang, Susan Jeffries, Mary F Lesch, Lucinda A Simmons, Santosh K Verma, and Joanna L Willetts. 2019. Employee acceptance of wearable technology in the workplace. *Applied ergonomics* 78 (2019), 148–156.
- [46] Wenjun Jiang, Chenglin Miao, Fenglong Ma, Shuochao Yao, Yaqing Wang, Ye Yuan, Hongfei Xue, Chen Song, Xin Ma, Dimitrios Koutsonikolas, et al. 2018. Towards environment independent device free human activity recognition. In *Proceedings of the 24th annual international conference on mobile computing and networking*. ACM, 289–304.
- [47] Bryce Kellogg, Vamsi Talla, and Shyamnath Gollakota. 2014. Bringing gesture recognition to all devices. In *11th USENIX Symposium on Networked Systems Design and Implementation (NSDI 14)*. 303–316.
- [48] Emily W Lam and Thomas DC Little. 2018. Refining light-based positioning for indoor smart spaces. In *Proceedings of the 4th ACM MobiHoc Workshop on Experiences with the Design and Implementation of Smart Objects*. 1–8.
- [49] Isah A Lawal and Sophia Bano. 2019. Deep human activity recognition using wearable sensors. In *Proceedings of the 12th ACM International Conference on Pervasive Technologies Related to Assistive Environments*. 45–48.
- [50] Dong Li, Shirui Cao, Sunghoon Ivan Lee, and Jie Xiong. 2022. Experience: practical problems for acoustic sensing. In *Proceedings of the 28th Annual International Conference on Mobile Computing and Networking*. 381–390.
- [51] Dong Li, Jialin Liu, Sunghoon Ivan Lee, and Jie Xiong. 2022. LASense: Pushing the Limits of Fine-grained Activity Sensing Using Acoustic Signals. *Proceedings of the ACM on Interactive, Mobile, Wearable and Ubiquitous Technologies* 6, 1 (2022), 1–27.
- [52] Huining Li, Chenhan Xu, Aditya Singh Rathore, Zhengxiong Li, Hanbin Zhang, Chen Song, Kun Wang, Lu Su, Feng Lin, Kui Ren, et al. 2020. VocalPrint: exploring a resilient and secure voice authentication via mmWave biometric interrogation. In *Proceedings of the 18th Conference on Embedded Networked Sensor Systems*. ACM, 312–325.
- [53] Tianhong Li, Lijie Fan, Mingmin Zhao, Yingcheng Liu, and Dina Katabi. 2019. Making the invisible visible: Action recognition through walls and occlusions. In *Proceedings of the IEEE/CVF International Conference on Computer Vision*. 872–881.
- [54] Chen Liu, Jie Xiong, Lin Cai, Lin Feng, Xiaojiang Chen, and Dingyi Fang. 2019. Beyond respiration: Contactless sleep sound-activity recognition using RF signals. *Proceedings of the ACM on Interactive, Mobile, Wearable and Ubiquitous Technologies* 3, 3 (2019), 1–22.
- [55] Tiantian Liu, Ming Gao, Feng Lin, Chao Wang, Zhongjie Ba, Jinsong Han, Wenyao Xu, and Kui Ren. 2021. Wavoice: A noise-resistant multi-modal speech recognition system fusing mmwave and audio signals. In *Proceedings of the 19th ACM Conference on Embedded Networked Sensor Systems*. ACM, 97–110.
- [56] Chris Xiaoxuan Lu, Stefano Rosa, Peijun Zhao, Bing Wang, Changhao Chen, John A Stankovic, Niki Trigoni, and Andrew Markham. 2020. See through smoke: robust indoor mapping with low-cost mmwave radar. In *Proceedings of the 18th International Conference on Mobile Systems, Applications, and Services*. 14–27.
- [57] Snehasis Mukherjee, Leburu Anvitha, and T Mohana Lahari. 2020. Human activity recognition in RGB-D videos by dynamic images. *Multimedia Tools and Applications* 79, 27 (2020), 19787–19801.
- [58] Ramon Nitzberg. 1972. Constant-false-alarm-rate signal processors for several types of interference. *IEEE Trans. Aerospace Electron. Systems* 1 (1972), 27–34.
- [59] Farzan M Noori, Md Zia Uddin, and Jim Torresen. 2021. Ultra-wideband radar-based activity recognition using deep learning. *IEEE Access* 9 (2021), 138132–138143.
- [60] Sameera Palipana, Dariush Salami, Luis A Leiva, and Stephan Sigg. 2021. Pantomime: Mid-air gesture recognition with sparse millimeter-wave radar point clouds. *Proceedings of the ACM on Interactive, Mobile, Wearable and Ubiquitous Technologies* 5, 1 (2021), 1–27.
- [61] Jacopo Pegoraro and Michele Rossi. 2021. Real-time people tracking and identification from sparse mm-wave radar point-clouds. *IEEE Access* 9 (2021), 78504–78520.
- [62] Swadhin Pradhan, Eugene Chai, Karthikeyan Sundaresan, Lili Qiu, Mohammad A. Khojastepour, and Sampath Rangarajan. 2017. RIO: A Pervasive RFID-based Touch Gesture Interface. In *Proceedings of the 23rd Annual International Conference on Mobile Computing and Networking (Snowbird, Utah, USA) (MobiCom '17)*. 261–274.
- [63] Sandeep Rao. 2017. Introduction to mmWave sensing: FMCW radars. *Texas Instruments (TI) mmWave Training Series* (2017), 1–11.
- [64] S Rao. 2020. Introduction to mmwave radar sensing: Fmcw radars. *Texas Instruments* (2020), 1–70.
- [65] Reuters. 2022. Tesla will remove more vehicle sensors amid Autopilot scrutiny. <https://auto.economictimes.indiatimes.com/news/passenger-vehicle/cars/tesla-will-remove-more-vehicle-sensors-amid-autopilot-scrutiny/9456463> [Accessed September 22, 2023].
- [66] Muhammad Moid Sandhu, Sara Khalifa, Kai Geissdoerfer, Raja Jurdak, and Marius Portmann. 2021. SoLAR: Energy positive human activity recognition using solar cells. In *2021 IEEE International Conference on Pervasive Computing and Communications (PerCom)*. IEEE, 1–10.

- [67] Mark C Schall Jr, Richard F Sese, and Lora A Cavuoto. 2018. Barriers to the adoption of wearable sensors in the workplace: A survey of occupational safety and health professionals. *Human factors* 60, 3 (2018), 351–362.
- [68] Ole Schumann, Markus Hahn, Jürgen Dickmann, and Christian Wöhler. 2018. Semantic segmentation on radar point clouds. In *2018 21st International Conference on Information Fusion (FUSION)*. IEEE, 2179–2186.
- [69] Argha Sen, Anirban Das, Prasenjit Karmakar, and Sandip Chakraborty. 2023. mmAssist: Passive Monitoring of Driver's Attentiveness Using mmWave Sensors. In *2023 15th International Conference on COMMunication Systems & NETWORKS (COMSNETS)*. IEEE, 545–553.
- [70] Argha Sen, Avijit Mandal, Prasenjit Karmakar, Anirban Das, and Sandip Chakraborty. 2023. mmDrive: mmWave Sensing for Live Monitoring and On-Device Inference of Dangerous Driving. In *2023 IEEE International Conference on Pervasive Computing and Communications (PerCom)*. IEEE, 2–11.
- [71] Xian Shuai, Yulin Shen, Yi Tang, Shuyao Shi, Luping Ji, and Guoliang Xing. 2021. millieye: A lightweight mmwave radar and camera fusion system for robust object detection. In *Proceedings of the International Conference on Internet-of-Things Design and Implementation*. 145–157.
- [72] Karen Simonyan and Andrew Zisserman. 2014. Very deep convolutional networks for large-scale image recognition. *arXiv preprint arXiv:1409.1556* (2014).
- [73] Akash Deep Singh, Sandeep Singh Sandha, Luis Garcia, and Mani Srivastava. 2019. Radhar: Human activity recognition from point clouds generated through a millimeter-wave radar. In *Proceedings of the 3rd ACM Workshop on Millimeter-wave Networks and Sensing Systems*. ACM, 51–56.
- [74] Elahe Soltanaghaei, Rahul Anand Sharma, Zehao Wang, Adarsh Chittilappilly, Anh Luong, Eric Giler, Katie Hall, Steve Elias, and Anthony Rowe. 2020. Robust and practical WiFi human sensing using on-device learning with a domain adaptive model. In *Proceedings of the 7th ACM International Conference on Systems for Energy-Efficient Buildings, Cities, and Transportation*. 150–159.
- [75] Sheng Tan, Linghan Zhang, Zi Wang, and Jie Yang. 2019. MultiTrack: Multi-user tracking and activity recognition using commodity WiFi. In *Proceedings of the 2019 CHI Conference on Human Factors in Computing Systems*. 1–12.
- [76] Arthur Venon, Yohan Dupuis, Pascal Vasseeur, and Pierre Merriaux. 2022. Millimeter Wave FMCW RADARs for Perception, Recognition and Localization in Automotive Applications: A Survey. *IEEE Transactions on Intelligent Vehicles* 7, 3 (2022), 533–555.
- [77] Chao Wang, Feng Lin, Tiantian Liu, Kaidi Zheng, Zhibo Wang, Zhengxiong Li, Ming-Chun Huang, Wenyao Xu, and Kui Ren. 2022. mmEve: eavesdropping on smartphone's earpiece via COTS mmWave device. In *Proceedings of the 28th Annual International Conference on Mobile Computing And Networking*. ACM, 338–351.
- [78] Guanhua Wang, Yongpan Zou, Zimu Zhou, Kaishun Wu, and Lionel M Ni. 2014. We can hear you with Wi-Fi!. In *Proceedings of the 20th annual international conference on Mobile computing and networking*. 593–604.
- [79] Lei Wang, Tao Gu, Wei Li, Haipeng Dai, Yong Zhang, Dongxiao Yu, Chenren Xu, and Daqing Zhang. 2023. DF-Sense: Multi-user Acoustic Sensing for Heartbeat Monitoring with Dualforming. In *Proceedings of the 21st Annual International Conference on Mobile Systems, Applications and Services*. 1–13.
- [80] Tianben Wang, Daqing Zhang, Yuanqing Zheng, Tao Gu, Xingshe Zhou, and Bernadette Dorizzi. 2018. C-FMCW based contactless respiration detection using acoustic signal. *Proceedings of the ACM on Interactive, Mobile, Wearable and Ubiquitous Technologies* 1, 4 (2018), 1–20.
- [81] Wei Wang, Alex X Liu, Muhammad Shahzad, Kang Ling, and Sanglu Lu. 2015. Understanding and modeling of wifi signal based human activity recognition. In *Proceedings of the 21st annual international conference on mobile computing and networking*. 65–76.
- [82] Yuheng Wang, Haipeng Liu, Kening Cui, Anfu Zhou, Wensheng Li, and Huadong Ma. 2021. m-activity: Accurate and real-time human activity recognition via millimeter wave radar. In *ICASSP 2021-2021 IEEE International Conference on Acoustics, Speech and Signal Processing (ICASSP)*. IEEE, 8298–8302.
- [83] Yanwen Wang and Yuanqing Zheng. 2018. Modeling RFID signal reflection for contact-free activity recognition. *Proceedings of the ACM on Interactive, Mobile, Wearable and Ubiquitous Technologies* 2, 4 (2018), 1–22.
- [84] Teng Wei and Xinyu Zhang. 2015. mtrack: High-precision passive tracking using millimeter wave radars. In *Proceedings of the 21st Annual International Conference on Mobile Computing and Networking*. ACM, 117–129.
- [85] Wikipedia. [n. d.]. Amazon Echo. https://en.wikipedia.org/wiki/Amazon_Echo
- [86] Jiahong Xie, Hao Kong, Jiadi Yu, Yingying Chen, Linghe Kong, Yanmin Zhu, and Feilong Tang. 2023. mm3DFace: Nonintrusive 3D Facial Reconstruction Leveraging mmWave Signals. In *Proceedings of the 21st Annual International Conference on Mobile Systems, Applications and Services*. 462–474.
- [87] Zhicheng Yang, Parth H Pathak, Yunze Zeng, Xixi Liran, and Prasant Mohapatra. 2016. Monitoring vital signs using millimeter wave. In *Proceedings of the 17th ACM international symposium on mobile ad hoc networking and computing*. ACM, 211–220.
- [88] Chengxi Yu, Zhezhuang Xu, Kun Yan, Ying-Ren Chien, Shih-Hau Fang, and Hsiao-Chun Wu. 2022. Noninvasive human activity recognition using millimeter-wave radar. *IEEE Systems Journal* (2022).
- [89] Jih-Tsun Yu, Li Yen, and Po-Hsuan Tseng. 2020. mmWave radar-based hand gesture recognition using range-angle image. In *2020 IEEE 91st Vehicular Technology Conference (VTC2020-Spring)*. IEEE, 1–5.
- [90] Bo Zhang, Boyu Jiang, Rong Zheng, Xiaoping Zhang, Jun Li, and Qiang Xu. 2023. Pi-ViMo: Physiology-inspired Robust Vital Sign Monitoring using mmWave Radars. *ACM Transactions on Internet of Things* 4, 2 (2023), 1–27.
- [91] Fusang Zhang, Jie Xiong, Zhaoxin Chang, Junqi Ma, and Daqing Zhang. 2022. Mobi2Sense: empowering wireless sensing with mobility. In *Proceedings of the 28th Annual International Conference on Mobile Computing And Networking*. 268–281.
- [92] Yang Zhang, Gierad Laput, and Chris Harrison. 2018. Vibrosight: Long-range vibrometry for smart environment sensing. In *Proceedings of the 31st Annual ACM Symposium on User Interface Software and Technology*. 225–236.
- [93] Mingmin Zhao, Tianhong Li, Mohammad Abu Alsheikh, Yonglong Tian, Hang Zhao, Antonio Torralba, and Dina Katabi. 2018. Through-wall human pose estimation using radio signals. In *Proceedings of the IEEE Conference on Computer Vision and Pattern Recognition*. 7356–7365.
- [94] Peijun Zhao, Chris Xiaoxuan Lu, Jianan Wang, Changhao Chen, Wei Wang, Niki Trigoni, and Andrew Markham. 2019. mid: Tracking and identifying people with millimeter wave radar. In *2019 15th International Conference on Distributed Computing in Sensor Systems (DCOSS)*. IEEE, 33–40.
- [95] Tianyue Zheng, Zhe Chen, Jun Luo, Lin Ke, Chaoyang Zhao, and Yaowen Yang. 2021. SiWa: see into walls via deep UWB radar. In *Proceedings of the 27th Annual International Conference on Mobile Computing and Networking*. 323–336.